

PREPARATION OF LCLS-II 1.3 GHZ PROTOTYPE CRYOMODULE TESTING AT FERMILAB*

K. Sirorattanakul[†], Lehigh University, Bethlehem, PA, USA
E. Harms, Fermi National Accelerator Laboratory, Batavia, IL, USA

Abstract

Linac Coherent Light Source II (LCLS-II) is a next generation x-ray free electron laser to be constructed in SLAC National Accelerator Laboratory's existing tunnel. The first prototype 1.3 GHz cryomodule was delivered to Fermilab's Cryomodule Testing Facility (CMTF) from Fermilab's Technical division on July 20, 2016 for testing. In preparation for the testing, we analyze the performance of testing facility's RF system, as well as develop necessary graphical interfaces to monitor the test. Results from test runs using test loads reveal that complete calibrations for power measurements are still needed for multiple cavities. In the meantime, the direct output from the amplifiers are stable with RMS less than 2 percent. It should be possible to make gradient calculations to within 5-10 percent.

INTRODUCTION

Linac Coherent Light Source (LCLS) is the world's first hard x-ray free electron laser located at SLAC National Accelerator Laboratory (SLAC), Menlo Park, CA, USA. Due to its success in operations since 2009, a major upgrade, Linac Coherent Light Source II (LCLS-II), is under development. With the upgrade to LCLS-II, the pulses for soft x-ray (energy < 5 keV) can be created at a rate of up to 929 kHz. However, for hard x-ray, it will maintain the rate of 120 Hz, but the operational range will extend from its current limit of 11 keV to 25 keV. LCLS-II is planned to be completed and have its first operation in January 2020 [1].

As one of the LCLS-II partner laboratories, Fermi National Accelerator Laboratory (Fermilab) is responsible for designing the cryomodules for the main linac. Together with Thomas Jefferson National Accelerator Facility (Jefferson lab), it is also responsible for building and test all the cryomodules, 17 by Fermilab and 18 by Jefferson lab. The main linac composes of thirty-five 1.3 GHz cryomodules and two 3.9 GHz bunch linearizing cryomodules. They are expected to work together to accelerate electrons to 4 GeV.

The first two 1.3 GHz cryomodules, one from each lab, are designated to be prototype cryomodules (pCMs). pCMs will be studied and tested more thoroughly than the subsequent production cryomodules to ensure a robust design that meets specifications. Changes in design and assembling procedures could be invoked as necessary.

CRYOMODULE DESIGN

The pCMs will be the first of their kind to run in continuous wave (CW) operation. The design of the LCLS-II cryomodules is largely based on the XFEL design with modifications to support CW operation. Each cryomodule consists of eight nine-cell TESLA-style superconducting accelerating cavities made from Niobium. A picture of a single cavity is shown in Fig. 1 and a rendering of the pCM showing external components is shown in Fig. 2. The cryomodule also contains a set of magnets for beam corrections, including one quadrupole and two dipoles, and a beam position monitor (BPM). It has the total length of 11.9189 m with a diameter of around 1.5 m [2, 3].



Figure 1: A nine-cell TESLA-style superconducting cavity in the clean room at Fermilab's Technical Division.

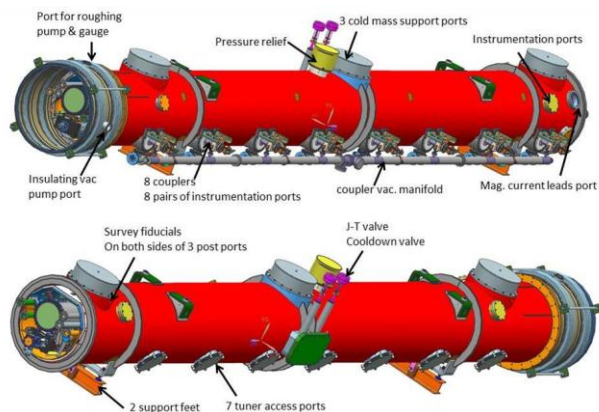


Figure 2: pCM and its external components [4].

CRYOMODULE TESTING

Superconducting accelerating cavities, such as those in LCLS-II cryomodules, must be tested at their operating temperature, which is around 2 Kelvin. At this temperature, not only that superconductor becomes superconducting, but the helium used to cool down also become superfluid. At Fermilab, the Cryomodule Testing Facility

* Work supported by Illinois Accelerator Institute through Lee Teng Undergraduate Fellowship in Accelerator Science and Engineering (summer 2016) and Fermi National Accelerator Laboratory.

[†] Email: krittanon.pond@gmail.com

(CMTF) was built for that purpose. The facility houses a cryogenic plant with 500W of cooling power at 2 Kelvin and two test stands. The first test stand, CMTS1, was built to support testing for both LCLS-II 1.3 GHz and 3.9 GHz cryomodules. CMTS1 commissioning began in July 2016 as the first LCLS-II pCM is readied for testing [5]. Fig. 3 shows the pCM installed in CMTS1.



Figure 3: pCM installation in CMTS1.

The testing at CMTF aims to characterize both the cryomodule's and each cavity's performance to ensure that they meet the stringent minimum acceptance criteria set by LCLS-II collaboration before delivery. There are over 20 parameters to be measured including usable gradient, intrinsic quality factor, heat load, connection between cryogenic and RF system, magnetic operational effect and shielding, to name a few [6]. Testing Fermilab pCM is expected to require 90 days, which will also include the studies of effect from the cooldown rate on its performance. Moving forward to test the production cryomodules, the testing period will be condensed to 28 days per cryomodule in order to meet the construction schedule of LCLS-II.

As we prepare for the test, we will analyze the performances of CMTS1's RF system, which will be turned on for this first time during this testing. We will characterize

the calibrations status of the power readouts as well as the precision of the power measurements as they will affect the gradient (E_{acc}) calculation. Two separate methods will be used to calculate the gradient to ensure the accuracy of the measurements and calculations.

The first method makes use of the probe (or transmitted) power (P_{probe}) measured by the antennas located at the end of each cavity and the external quality factor (Q_2) calculated from the decay time measurement as shown in Eq. 1.

$$E_{acc} = \sqrt{P_{probe} Q_2 \frac{(r/Q)}{L}} \quad (1)$$

The second method makes use of the forward power from the external system ($P_{forward}$) and the intrinsic quality factor (Q_0) calculated from the heat load as shown in Eq. 2.

$$E_{acc} = \sqrt{4P_{forward} Q_0 \frac{(r/Q)}{L}} \quad (2)$$

For both methods, the geometric shunt impedance (r/Q) and the electrical length (L) can be determined with almost negligible errors [7]. The error of the gradient calculations then lies in the error of the powers and the error of the quality factors.

RF SYSTEM LAYOUT

The RF power system of CMTS1 consists of eight 4kW solid state amplifiers (SSAs) from R&K company limited; each powers one cavity. The power from each amplifier is transmitted through a set of rectangular waveguides, passing through two directional couplers, and an isolator as shown in Fig. 4. One of the two directional couplers located just before the isolator, while another directional coupler located before entering the cavity. The isolator's function is to minimize the power loss through the waveguides system. All the waveguides, including isolators, bends, and couplers are made by Mega Industries, LLC.

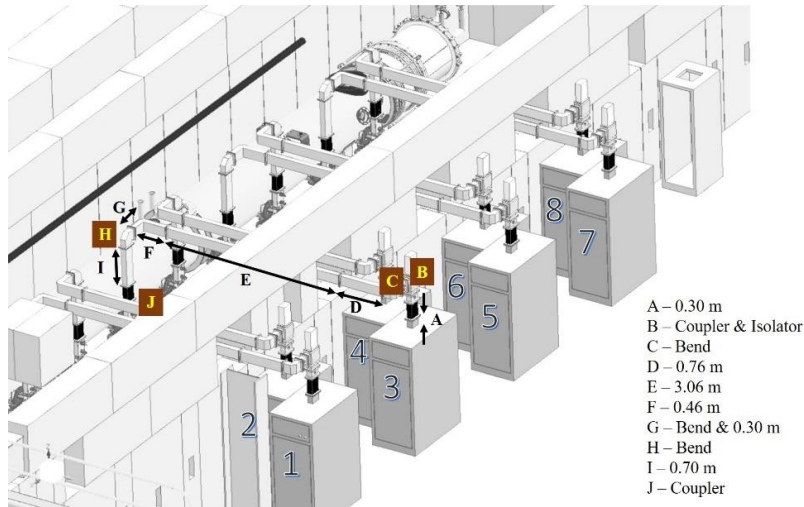


Figure 4: CMTS1's RF system layout.

Table 1: Calculated power losses through each section of the RF system

Sections	A	B	C	D	E	F	G	H	I	J	Total Loss
1, 3, 5, 7	0.06%	1.21%	0.01%	0.14%	0.58%	0.09%	0.08%	0.01%	0.13%	0.06%	2.37%
2, 4, 6, 8	0.06%	1.21%	0.01%	-	0.58%	0.09%	0.08%	0.01%	0.13%	0.06%	2.23%

To monitor the system, forward and reflected (or reversed) powers will be measured for each cavity at the amplifiers, the isolators, and at a directional coupler immediately in front of each cavity fundamental power coupler. The probe power at the end of the cavity will also be measured. The powers will be readout to Fermilab's Accelerator Control System (ACNET). A sample interface of ACNET is shown in Fig. 5. The default acquisition rate for the powers is 1 Hz, but can be increased to up to 10 kHz when capturing waveforms.

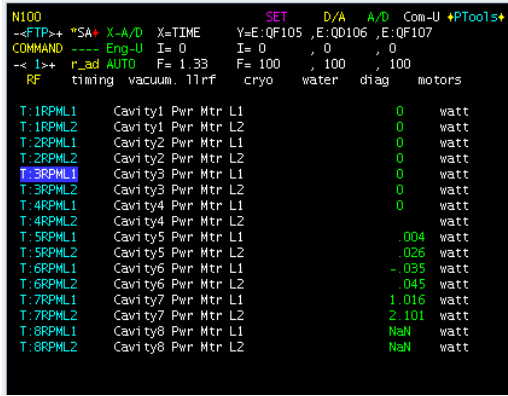


Figure 5: Sample interface of Fermilab's ACNET system.

RF SYSTEM ANALYSIS

Power calibrations

To determine whether the power meters are well-calibrated, we will compare the calculated values from theory with the measured values from the test runs using test loads. This work will focus on power calibrations for the meters located at the amplifiers and at the directional coupler just before entering the cavity (also referred to as low-level RF: LLRF).

For the straight sections of rectangular waveguides with the dimensions of a and b , where a is greater than b , power attenuation for TE₁₀ mode in dBm/m is predicted by the following equation [8]:

$$\alpha_c = 8.686 \frac{R_s}{\eta b} \frac{1 + (2b/a)(\omega_c^2/\omega^2)}{\sqrt{1 - \omega_c^2/\omega^2}} \quad (3)$$

where the surface resistance, $R_s = \sqrt{\omega\mu/2\sigma}$; the impedance, $\eta = \sqrt{\mu/\epsilon}$; and the critical frequency, $\omega_c = c\pi/a$.

At CMTS1, the straight sections of the waveguides are model WR-650 manufactured by Mega Industries, LLC from Aluminum 6061-T6, which have the electrical conductivity (σ) of 2.506×10^7 Siemens/m. In this case, $a = 6.5$ inches and $b = 3.25$ inches. We approximate that

permittivity (ϵ) of normal air as well as the permeability (μ) of air are the same as that of the free space. We calculate the surface resistance, R_s , to be 1.43×10^{-2} Ohms; the impedance, η , to be $3.77 \times 10^2 \text{ m}^2 \text{ kg s}^{-3} \text{ A}^{-2}$; and the critical angular frequency, ω_c , to be $5.71 \times 10^9 \text{ rad/s}$. With all these parameters, the attenuation is $8.32 \times 10^{-3} \text{ dBm/m}$.

By using Eq. 4, derived from the conversion between dBm and Watts shown in appendix A, we can calculate the attenuation in the straight sections of CMTS1 waveguides to be 0.19%/m.

$$P_{\text{loss}}(\%) = (10^{P_{\text{loss}}(\text{dBm})/10} - 1) \times 100 \quad (4)$$

Attenuation in the bends and the couplers is harder to precisely predict by the theory. Here, we use the specifications of voltage standing wave ratio (VSWR) from the company to estimate the attenuation. The VSWR can be converted to power loss in percent by using Eq. 5 [9].

$$\text{Power loss}(\%) = \left(\frac{\text{VSWR} - 1}{\text{VSWR} + 1} \right)^2 \times 100 \quad (5)$$

In miter bends, the VSWR is 1.02:1 [10], while in directional couplers, the VSWR for the main arm is 1.05:1 and for the side arm is 1.25:1 [11]. The power gets transmitted via the side arm for the coupler next the isolator, while it gets transmitted via the main arm for the coupler next to the cavity.

It turns out that the total losses between the amplifiers and the cavities are 2.37% for amplifiers number 1, 3, 5, and 7 and 2.22% for amplifiers number 2, 4, 6, and 8 (see Table 1 for section-by-section calculations). The difference between the calculated losses from the two sets are the missing sections, labelled D in Fig. 4.

We compare these theoretical calculations with the results from the test runs using test loads. The start and end time for the test runs for five amplifiers SSAs are shown in Table 2.

Table 2: Selected start and end time for test runs analysis

SSA #	Start Time		End Time	
2	07-06-2016	07:30	07-08-2016	09:15
3	07-22-2016	11:45	07-22-2016	13:15
5	07-22-2016	09:18	07-22-2016	09:54
6	07-14-2016	18:00	07-15-2016	10:00
7	07-21-2016	17:15	07-21-2016	08:00

The measured attenuation between the amplifiers and the cavities are shown in Table 3. Results show that the measure losses are greater than the calculated losses as one would expect. SSA number 2 is well-calibrated since the measured and calculated losses agree really well with each other, within 0.5%. However, the calculated and

measured attenuation for SSA number 3, 5, 6, and 7 do not agree with each other, which shows that complete calibrations are still needed for these amplifiers. Calibration procedures used for SSA number 2 should be adopted for future calibrations.

Table 3: Calculated power loss and measured power loss from the test runs for 5 SSAs

SSA Number	2	3	5	6	7
Output (W)	668.1	2195	2107	1539	1055
Calc. loss (%)	2.22	2.37	2.37	2.22	2.37
Meas. Loss (%)	2.22	6.01	6.90	7.73	6.13

Performance of the Amplifiers

As we move on from calibrations to real analysis, we need to ensure that the output from the amplifiers is stable over an extended period of time. Due to the current acquisition method, the outputs are only in integers. This creates an obstacle to study the waveforms that the outputs might exhibit.

We impose the technique of binning average to recover the waveform. We do this by dividing the data into bins of n data points. The first data point of the new set will be the average of first n data points. The second data point of the new set will be the average from the second to the $n+1$ th data points, and so on. We compare the results from different values of n with the forward power at the cavity. We know that propagation through waveguides will attenuate the power, but should preserve the waveforms. We do the similar analysis for all the amplifiers with test runs and found out that the n of 50 data points is the best value for doing this waveform recovery. The sample time series plot showing the recovery of the waveforms for SSA number 2 is shown in Fig. 6. The plots on the top are the powers measured at SSA number 6. The left one is the raw output, while the right one is after waveform recovery with 50 data points per bin. The plot at the bottom is the time series for the power measured at the cavity.

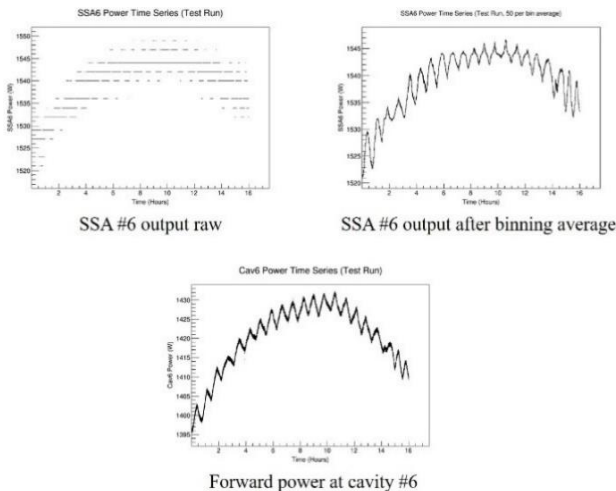


Figure 6: Time series showing waveform recovery.

After imposing waveform recovery, we analyse the stability of the data from the test runs by determining the RMS values of the output from the amplifiers. The results are shown in Table 4. Histogram and time series for each test run are documented in appendix B.

In the longer runs over a few hours, we observe that the systems exhibit the undesired oscillations in electronics, known as parasitic oscillations. Some of them seem to exhibit higher-order oscillations with longer period in order of around a day. However, the length of the test runs is not long enough to quantify this periodicity.

To improve the accuracy of periodicity analysis, we eliminate the disturbances from higher-order oscillations. We model the higher-order oscillations by using a median fit. This is similar to the binning average, but instead of finding the average of the bin, we find the median of the bin. The bin size used for determining the median is ~ 2.78 hour or 10,000 data points.

After determining the median fit, we subtract the median fit model from the values of the raw data. We then run the residuals from the subtractions through Lomb-Scargle algorithm implemented in the VARTOOLS light curve analysis program to search for a period of the parasitic oscillations [12-14]. The summary of the analysis is shown in Table 4 along with the RMS values.

Table 4: SSA output statistics.

SSA Number	2	3	5	6	7
Mean power (W)	668.1	2195	2107	1539	1055
Duration (hrs)	49.75	1.5	0.6	16	14.75
Power RMS (%)	2.08	0.28	0.15	0.36	0.50
Period (hrs)	0.79	-	-	0.79	0.78

The results from the analysis show that the output from the amplifiers are stable with RMS less than 2 percent during continuous operation up to two days duration. For longer runs that exhibit the parasitic oscillations, we found that the periods of the oscillations are similar to each other at around 0.8 hour, which means that they are likely to be resulting from systematics.

From this analysis, we want to quantify the error of gradient calculation. The propagation of error for the first method from the probe power is shown in Eq. 6 (derivation shown in appendix A).

$$\frac{\Delta E_{acc}}{E_{acc}} = \frac{1}{2} \cdot \frac{\Delta P_{probe}}{P_{probe}} \quad (6)$$

The propagation of error for the second method from the forward power is shown in Eq. 7 (derivation shown in appendix A).

$$\frac{\Delta E_{acc}}{E_{acc}} = \frac{1}{2} \cdot \frac{\Delta P_{forward}}{P_{forward}} \quad (7)$$

The error of the power measurement of both the forward power and the probe power can be estimated to be the RMS value of the output from the amplifiers. With the RMS of 2 percent, the first method of gradient calculation

will propagate the error of around 1 percent, as well as the second method. These errors are in the range that is tolerable for cavities testing. With careful measurement of the quality factor, we should be able to determine the gradient to within 5-10 percent.

INTERFACES DEVELOPMENT

LabVIEW Power Readouts

There are certain tests, such as determining the coupling conditions, which require analysis of the waveform. For power readouts, we will use a LabVIEW interface to readout the value as well as displaying the waveform in real-time as shown in Fig 7. The first page on the left allows one to set the offset (dBm) for the readouts as well as display the device name in ACNET, the serial number of the meter, and the readout itself. The second page in the middle allows one to display the time plot of the readouts. The third page on the right allows one to set the acquisition settings such as measurement rate, units, and frequency. This program was first developed by David Slimmer. We modified and added some functions, including frequency settings and offset settings, to the existing program (see appendix C for the main page of the program's source code).

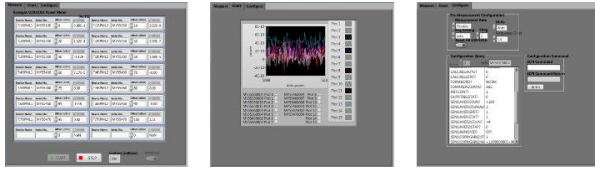


Figure 7: LabVIEW interface for power readouts.

Synoptic Displays

In order to ensure that the testing runs smoothly, we need to keep track of important parameters, such as powers, temperatures and external magnetic fields, real-time. This will be done through the graphical interfaces developed using a Fermilab-developed synoptic display platform. The program will communicate with ACNET to acquire real-time data.

Fig. 8 shows a sample synoptic display. This particular display shows power readouts from different locations in the system. The status of the amplifiers is shown as On (green) or Off (red). Clicking "Detailed powers" will link to powers display for individual cavity which will also include time plot of the powers.

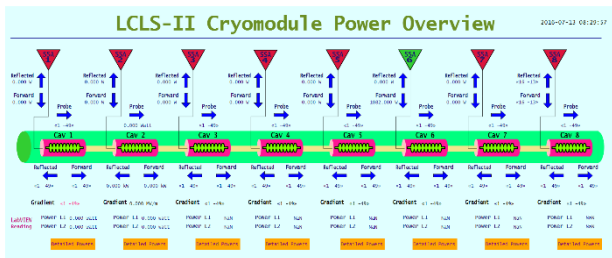


Figure 8: Synoptic display of different power readouts.

CONCLUSIONS

As we analyze the RF system of CMTS1, we found that SSA number 2 is well calibrated. SSA number 3, 5, 6, and 7 still need complete calibration with the same procedure used for SSA number 2. On the other hand, all of their outputs are stable for continuous operations up to two days duration with RMS less than 2 percent. This contributes only 1-2 percent error to gradient calculation. With careful measurement of the quality factor, we should be able to determine the gradient to within 5-10 percent.

We also successfully developed the necessary graphical interfaces to record the waveform of the power readouts via LabVIEW, as well as to display the important parameters real-time via synoptic display.

FUTURE PLANS

As we finishing up preparation work for the testing, it is planned to cool down the prototype cryomodule to 2 Kelvin around mid-August. Testing of the prototype will last until late 2016. As testing of the prototype wraps up in late 2016, Fermilab's Technical Division will start to build the first production cryomodule. The testing of the production cryomodule will start in the beginning of 2017 with a 28-day cycle per module.

ACKNOWLEDGMENT

This work will be impossible without valuable advices from my mentor, Elvin Harms, and funding from the Illinois Accelerator Institute through the Lee Teng Undergraduate Fellowship in Accelerator Science and Technology. I would also like to thank David Slimmer for his guidance and help on LabVIEW interface, Denise Finstrom, Linden Carmichael, and Dennis Nicklaus for their guidance on synoptic, as well as all the programs and libraries I used including LabVIEW, ROOT, synoptic, python (numpy, matplotlib), and the VARTOOLS light curve analysis program.

REFERENCES

- [1] LCLS-II Project Team, "LCLS-II Final Design Report DRAFT," SLAC, Menlo Park, CA, USA, Rep. LCLSII-1.1-DR-0251-R0, Dec. 2014.
- [2] T. Arkan *et al.*, "LCLS-II 1.3 GHz Design Integration for Assembly and Cryomodule Assembly Facility Readiness at Fermilab," in *Proc. 17th Int. Conf. on RF Superconductivity (SRF2015)*, Whistler, BC, Canada, Sep. 2015, paper TUPB110, pp. 893–897.
- [3] T. Peterson *et al.*, "LCLS-II Cryomodule Design – Modified TESLA-Style Cryomodule for CW Operation," in *Proc. 17th Int. Conf. on RF Superconductivity (SRF2015)*, Whistler, BC, Canada, Sep. 2015, paper THPB119, pp. 1417–1421.
- [4] Y. He *et al.*, "LCLS-II Prototype Cryomodule Interfaces," Fermilab, Batavia, IL, USA, Rep. ED0002307, Rev., Jan. 2015.
- [5] E. Harms *et al.*, "Fermilab Cryomodule Test Stand Design and Plans," in *Proc. 17th Int. Conf. on RF Superconductivity (SRF2015)*, Whistler, BC, Canada, Sep. 2015, paper TUPB013, pp. 566–570.

- [6] E. Harms, “Prototype Cryomodule Testing Plan,” presented at LCLS-II FAC Review, Fermilab, Batavia, IL, USA, Jul. 2016.
- [7] T. Powers, “Theory and Practice of Cavity RF Test Systems,” U.S. Particle Accelerator School (USPAS), 2011.
- [8] S. Orfanidis, “Chapter 9: Waveguides,” in *Electromagnetic Waves and Antennas*, New Brunswick, NJ, USA: Rutgers University, 2008, pp. 362–410.
- [9] P-N Designs, Inc. and IEEE, “VSWR Calculator,” Micro waves101.com,
[URL: <http://www.microwaves101.com/calculators/872-vswr-calculator>]
- [10] Mega Industries, LLC, “Miter Bends,” Product Data Sheet.
- [11] Mega Industries, LLC, “Waveguide Directional Couplers,” Product Data Sheet.
- [12] J. Hartman and G. Bakos, “Vartools: A program for analyzing astronomical time-series data,” *Astronomy and Computing*, vol. 17, pp. 1–72, Oct. 2016, to be published.
- [13] M. Zechmeister and M. Kurster, “The generalised Lomb-Scargle periodogram. A new formalism for the floating-mean and Keplerian periodograms,” *Astronomy and Astrophysics*, vol. 496, pp. 577–584, Jan. 2009.
- [14] W. Press, S. Teukolsky, W. Vetterling, and B. Flannery, *Numerical Recipes in C*. New York, USA: Cambridge University Press, 1992.

APPENDIX A: EQUATIONS DERIVATION

POWER LOSS CONVERSION FROM DBM TO % (EQ. 4)

The conversion from Watts to dBm is as follows:

$$P(\text{dBm}) = 10 \log P(W) + 30 \quad (8)$$

The conversion from dBm to Watts is as follows:

$$P(W) = 10^{(P(\text{dBm})-30)/10} \quad (9)$$

By using these two equations, we can convert the attenuation in dBm to percentage power loss in Watts as follows:

$$\begin{aligned} P_1(\text{dBm}) - P_2(\text{dBm}) &= [10 \log P_1(W) + 30] - [10 \log P_2(W) + 30] \\ &= 10 \log P_1(W) - 10 \log P_2(W) \\ &= 10 \log \frac{P_1(W)}{P_2(W)} \end{aligned} \quad (10)$$

Hence,

$$P_{\text{loss}}(\text{dBm}) = 10 \log \left(\frac{100 + P_{\text{loss}}(\%)}{100} \right) \quad (11)$$

By inverting Eq. 11, we recover Eq. 4.

ERROR PROPAGATION FOR GRADIENT MEASUREMENT (EQ. 6 AND 7)

We can calculate the error propagation by using derivative. For Eq. 6, we start from taking a derivative of Eq. 1.

$$\frac{dE_{\text{acc}}}{dP_{\text{probe}}} = \frac{1}{2} \cdot \left(P_{\text{probe}} Q_2 \frac{(r/Q)}{L} \right)^{-1/2} \cdot Q_2 \frac{(r/Q)}{L} \quad (12)$$

This can be reduced to

$$\frac{\Delta E_{\text{acc}}}{\Delta P_{\text{probe}}} = \frac{1}{2E_{\text{acc}}} \cdot \frac{E_{\text{acc}}^2}{P_{\text{probe}}} = \frac{E_{\text{acc}}}{2P_{\text{probe}}} \quad (13)$$

which can be further arranged to match with Eq. 6.

For Eq. 7, we start from taking a derivative of Eq. 2.

$$\frac{dE_{\text{acc}}}{dP_{\text{forward}}} = \frac{1}{2} \cdot \left(4P_{\text{forward}} Q_0 \frac{(r/Q)}{L} \right)^{-1/2} \cdot 4Q_0 \frac{(r/Q)}{L} \quad (14)$$

This can be reduced to

$$\frac{\Delta E_{\text{acc}}}{\Delta P_{\text{forward}}} = \frac{1}{2E_{\text{acc}}} \cdot \frac{E_{\text{acc}}^2}{P_{\text{forward}}} = \frac{E_{\text{acc}}}{2P_{\text{forward}}} \quad (15)$$

which can be further arranged to match with Eq. 7.

APPENDIX B: DETAILED PLOTS

Histograms

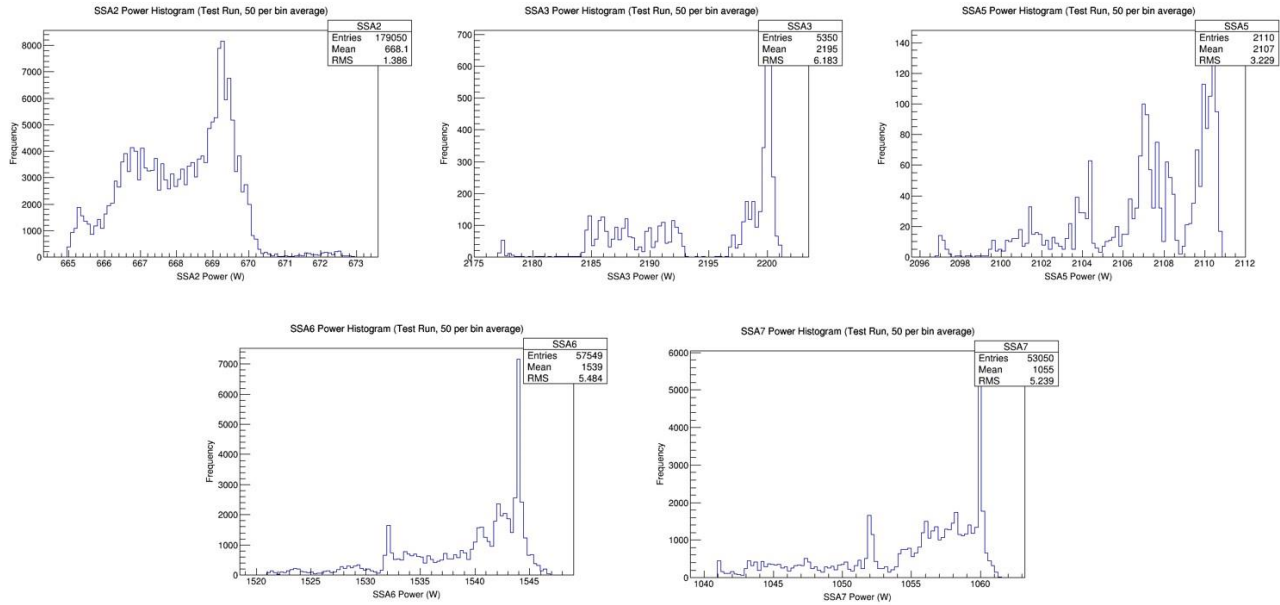


Figure 9: Histograms of output from the amplifiers.

Time Series

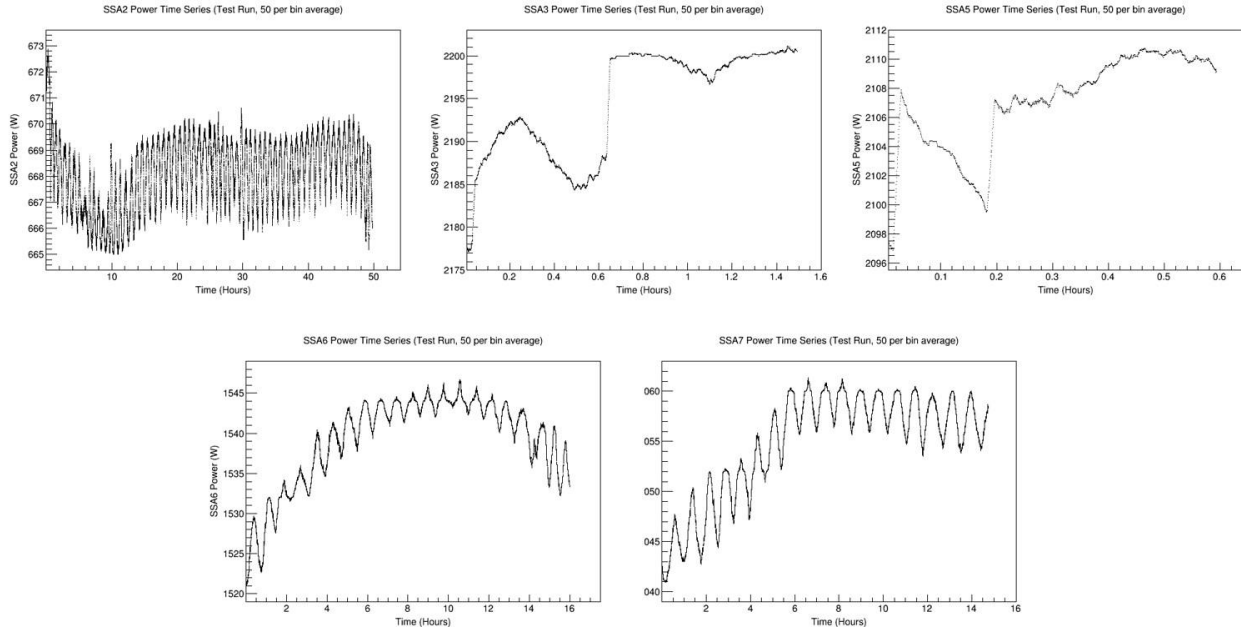


Figure 10: Time series of output from the amplifiers.

APPENDIX C: LABVIEW PROGRAM SOURCE CODE

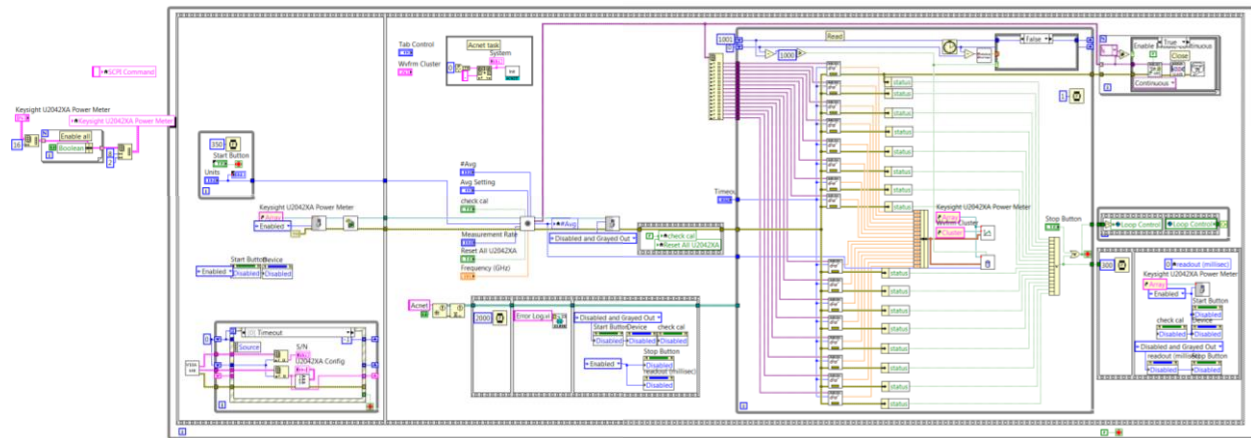


Figure 11: LabVIEW main program source code.